Enhanced Segmental Dynamics of Poly(lactic acid) Glasses during Constant Strain Rate Deformation

Journal:	*Macromolecules*
Manuscript ID	ma-2019-01363d.R1
Manuscript Type:	Article
Date Submitted by the Author:	n/a
Complete List of Authors:	Bennin, Trevor; University of Wisconsin Madison, Chemistry Ricci, Josh; University of Wisconsin Madison Graduate School, Chemistry Ediger, Mark; University of Wisconsin Madison, Chemistry

Enhanced Segmental Dynamics of Poly(lactic acid) Glasses during Constant Strain Rate Deformation

Trevor Bennin*, Josh Ricci, M. D. Ediger

Department of Chemistry, University of Wisconsin – Madison, Madison, Wisconsin 53706, United States

***Corresponding Author (tbennin@wisc.edu)**

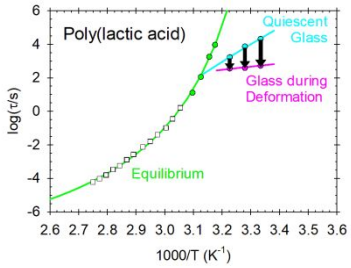

For Table of Contents use only

Abstract

The combined effects of temperature and deformation on the segmental dynamics of poly(lactic acid) (PLA) glasses were investigated using probe reorientation measurements. Constant strain rate deformations, with strain rates between 6×10^{-6} s^{-1} and 3×10^{-5} s^{-1}, were performed on PLA glasses at temperatures between T_g – 15 K and T_g – 25 K. Deformation decreases the segmental relaxation time by up to a factor of 30 relative to the undeformed state. The segmental

relaxation time in the post-yield regime is related to the local strain rate via a power-law, with exponents similar to those reported for lightly crosslinked PMMA. The Kohlrausch-Williams-Watts exponent, β_{KWW}, commonly interpreted in terms of the width of the distribution of segmental relaxation times, changes from the undeformed state to the post-yield regime, indicating a significant narrowing of the relaxation spectrum. We observe that β_{KWW} is correlated to the deformation-induced increase of segmental mobility for PLA, as was reported for PMMA. The similar responses of PLA and PMMA to deformation suggest that the observed effects are the generic consequences of constant strain rate deformation on the segmental dynamics of polymer glasses.

Introduction

Polymer glasses are important engineering materials due to their many useful properties, such as their ease of processability, macroscopic homogeneity, and mechanical toughness. In common with other glassy materials, the linear mechanical properties of polymer glasses depend on the time scale over which they are measured: at short times, they act as elastic solids, while at long times, they are able to flow like viscous liquids.[1, 2] The relevant time scale for this change in properties of polymer glasses is the segmental relaxation time, which is typically longer than experimental time scales below the glass transition temperature, T_g. A crossover between elastic solid-like properties and viscous liquid-like properties can also be observed in the nonlinear deformation of polymer glasses. For example, during constant strain rate deformation, a polymer glass transitions from an initial elastic response into a post-yield "flow" state, suggesting that the segmental relaxation time has accelerated in this process. In spite of decades of work, a fundamental description of the deformation of polymer glasses, in terms of the mechanical response and changes in segmental dynamics, has not been fully developed. This can be

attributed to the nonlinear nature of the deformation process and the amorphous structure of glasses. In contrast to crystals, the local structure and dynamics of glasses are highly heterogeneous,[3, 4] which prevents the use of defect-based models commonly used for crystalline materials[5, 6]. Additional aspects of polymer deformation, such as strain hardening and the brittle-ductile transition, can also be attributed to the unique chain structure of polymers.[7-9] An improved fundamental description of the deformation of polymer glasses will lead to a deeper understanding of the complex physics of glasses and to greater predictive power for the manufacturing of advanced materials.[6, 10, 11]

Many theoretical approaches have been taken to describe the deformation of polymer glasses. As early as 1936, Eyring used a barrier-hopping model to describe the plasticity of solid materials.[12] In his model, the stress imposed on a solid effectively decreased the height of barriers, allowing for faster molecular rearrangements and macroscopic flow. Models that employ a single relaxation time, like the fluidity model of Fielding, Larson and Cates,[13-15] the Eindhoven Glassy Polymer model[16] and Chen and Schweizer's nonlinear Langevin equation (NLE) theory,[17-19] have been used to describe nonlinear deformation even without explicitly including a distribution of relaxation times. Other models include, either implicitly or explicitly, a distribution of relaxation times to account for spatially heterogeneous dynamics. For example, the stochastic constitutive model (SCM) by Medvedev and Caruthers is a fully tensorial, mesoscopic model that has been used to describe physical aging and nonlinear deformation.[20] It predicts a distribution of relaxation times which allows for deformation-induced changes in the dynamic heterogeneity to be described. Alternatively, the percolation of free volume distribution (PFVD) model by Long and coworkers is also a mesoscopic model that incorporates a distribution of relaxation times. It is also able to describe physical aging[21] and nonlinear

deformation,[22] as well as changes in the dynamic heterogeneity of the system.[23] These models rely on a variety of different mechanisms to couple microscopic quantities (like density fluctuations, entropy fluctuations, and relaxation times) with macroscopic quantities (like stress and strain). While each model can effectively describe some aspects of the macroscopic mechanical response of a polymer glass to deformation, it is important to experimentally verify the underlying connection between the microscopic and macroscopic quantities. One important test for these models is to compare their predictions with measured changes in the segmental relaxation time of a glass in response to deformation.

Many simulations and experiments have been performed to learn about the segmental dynamics of polymer glasses during deformation. Simulations of polymer glass deformation can directly measure accelerated dynamics in polymer glasses by calculating microscopic quantities that are typically unavailable in experiments, like particle hopping rates,[24] bond autocorrelation functions,[25, 26] and intermediate scattering functions.[24, 25, 27, 28] Experimentally, mechanical testing[29, 30] has been used to infer changes in segmental dynamics during deformation.[31] NMR,[32] probe diffusion,[33] and dielectric spectroscopy[34, 35] all provide direct evidence for enhanced segmental dynamics during deformation. For one system, lightly crosslinked PMMA glasses, probe reorientation techniques have identified and quantified the changes in the segmental dynamics during constant stress (creep)[36-38] and constant strain rate deformations.[39, 40] In these probe reorientation experiments, it was shown that the relaxation time is strongly correlated with the strain rate in the plastic flow regime. It was also shown that deformation acts to narrow the distribution of segmental relaxation times, thus making the dynamics of a polymer glass more homogeneous. While the probe reorientation experiments have extensively characterized the segmental dynamics of lightly crosslinked PMMA during deformation, this system may not be

ideal for identifying the generic response of polymer glasses due to the presence of crosslinks[41, 42] and the existence of an overlapping secondary relaxation.[43, 44] Quantitative measurements of segmental dynamics during deformation of another polymer glass can help to determine the generality of the results of these previous experiments and provide additional quantitative data for the potential refinement of models of polymer glass deformation.

Here we perform probe reorientation experiments on a poly(lactic acid) glass during constant strain rate tensile deformation at various temperatures somewhat below T_g. Strain rates between 6×10^{-6} s^{-1} and 3×10^{-5} s^{-1} were utilized at temperatures ranging from T_g – 25 K to T_g – 15 K. The segmental dynamics were monitored during deformation using the probe reorientation technique. Parameters from the Kohlrausch-Williams-Watts function, τ_{KWW} and β_{KWW}, representative of the average segmental relaxation time and the width of the distribution of relaxation times, respectively, were collected at various temperatures and strain rates, enabling a comparison to previous measurements on lightly crosslinked PMMA.

We find that at the coldest temperatures and fastest strain rates investigated, the segmental dynamics of PLA glasses can be accelerated by up to a factor of 30 during constant strain rate deformation. We show that the relaxation times of PLA glasses in the plastic flow regime are related to the local strain rate via a power-law relationship and that the change in the plastic flow relaxation time with strain rate for PLA is very similar to that of lightly crosslinked PMMA glasses. We also find that the temperature dependence of the relaxation times for PLA and PMMA glasses in the plastic flow regime are the same. Finally, we find that the distribution of relaxation times for PLA narrows during deformation, similar to PMMA. These combined findings suggest that the observed effects are the generic response of polymer glasses undergoing constant strain rate deformation.

Experimental Methods

Sample Preparation. Films of atactic poly(lactic acid) (PLA) were solvent-cast using the following method. Poly(DL-lactide) pellets with M_n = 170 kg/mol, Đ = 1.05, and L/D ratio of 50/50 were purchased (AP164, Akina, Inc.) and used without further purification. 0.8 g of PLA pellets were dissolved in 10 mL of dichloromethane in a glass vial. The fluorescent probe N,N'-dipentyl-3,4,9,10-perylenedicarboximide (DPPC, Aldrich) was introduced to the solution to have a concentration between 10^{-7} M and 10^{-6} M in the resulting polymer film. The structure of atactic PLA and DPPC are shown below in Figure 1. The polymer/probe solution was filtered through a PTFE membrane with pore size 0.2 μm and transferred to flat-bottom glass dishes (diameter = 15 cm). The glass dishes were covered with aluminum foil in which a few small holes were punched to control the rate of evaporation. The solvent was evaporated over 24 hours at room temperature. The films were removed from the glass dishes via sonication and placed in an oven at 335 K for 24 hours to evaporate any remaining solvent. Samples were cut from the films using a custom-made steel die that conforms to a scaled-down "dog-bone" shape of ASTM D1708-10. The cut samples had average thicknesses between 35 and 55 μm. The glass transition temperature of the material, T_g, was measured to be 325 ± 1 K as determined via DSC using the midpoint of the transition of the second heating scan at 10 K/min.

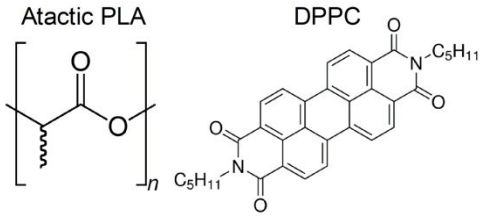

Figure 1. The structures of the polymer and probe used in this work, atactic PLA (left) and DPPC (right).

Deformation Apparatus. The custom-built deformation apparatus utilized here has been previously described.[39] The polymer sample is clamped into clips that are loaded into a temperature-controlled brass chamber. One clip is fixed in place while the other is attached to a

poly(ether imide) rod that extends beyond the brass chamber and connects to a 5 N load cell to monitor the force applied to the sample. The load cell is attached to a U-shaped aluminum bar which is moved by a linear actuator. The position and velocity of the linear actuator controls the extent and speed of the deformation. The bottom of the brass chamber is fitted with a glass window, and the entire deformation apparatus sits on top of a confocal microscope to allow for probe reorientation and local strain measurements during deformation.

Constant global strain rate deformation was performed by controlling the linear actuator velocity. The deformation of glassy polymers can occur inhomogeneously, so a distinction must be made between the applied global strain rate and the local strain rate at the location of the optical measurements. The local strain rate is not controlled but is broadly targeted by applying an appropriate global strain rate; it is measured independently by taking images of bleached lines within the approximately 500 μm × 500 μm local measurement area. The local strain rate is calculated using the change in the distance between the bleached lines between images. The local strain rate is typically equal to the global strain rate until yielding occurs, when strain localization occurs in the sample. After yield, the calculated local strain rate is effectively constant and larger than the applied global strain rate.[39] The amount by which the local strain rate becomes larger than the global strain rate depends on the inhomogeneity of the deformation (i.e. the extent of strain localization) and the position of the optical experiment, and can be up to a factor of 5. Representative plots of the local strain and global strain during deformation can be found in Figure S1.

Thermal Protocol. The free-standing sample, clamped in the sample clips, is placed in an oven set to 335 K (T_g + 10 K) for 15 minutes to eliminate its thermal and mechanical history. Next, the sample is removed from the oven and cooled to room temperature (T_g – 30 K). The

PLA sample is expected to rapidly cool through the glass transition, which has been reported to improve the ductility of PLA glasses.[45] The sample is loaded into the deformation instrument five minutes after being removed from the oven. Once loaded, the temperature of the sample is increased at 1 K/minute to the testing temperature, where the sample is then held isothermally for the remainder of the experiment. The sample is allowed to age for 30 minutes at the testing temperature before the deformation begins. The temperature accuracy of the apparatus is ±1 K, as determined by melting point tests. The temperature is stable to ±0.2 K during an experiment.

Probe Reorientation Measurements. Probe reorientation measurements were performed during active deformation, as previously described.[39, 40] The sample is briefly exposed to a linearly polarized 532 nm laser beam which preferentially photobleaches probes with transition dipoles aligned with the polarization of the beam. Then a weak, circularly polarized beam induces fluorescence of the remaining unbleached probes. The fluorescence intensities parallel and perpendicular to the polarization of the bleaching beam is monitored and compared to intensities of a reference unbleached location to measure the anisotropy, $r(t)$, as a function of time.

The time decay of the anisotropy can be described with the Kohlrausch-Williams-Watts (KWW) function:

$$r(t) = r(0)e^{-(t/\tau_{KWW})^{\beta_{KWW}}}$$

Here, $r(0)$ is the anisotropy immediately after the photobleaching event, τ_{KWW} is a characteristic segmental relaxation time, and β_{KWW} describes the nonexponentiality of the decay, which is commonly interpreted in terms of the width of the distribution of relaxation times. Anisotropy data is fitted with a KWW function to extract τ_{KWW} and β_{KWW}, which are presented in this work.

Previous work has shown that DPPC, used here in PLA, is a good reporter of segmental dynamics in lightly crosslinked PMMA melts[37] and glasses[46] in the absence of deformation.

Because the measurement of probe reorientation is not instantaneous, our probe reorientation times report an effective relaxation time that averages over a small range of strains. Measurements very near to the yield strain average over pre-yield and post-yield mobility, giving a relaxation time longer than the plateau value (as seen below in Figure 7). The plateau relaxation time is measured reproducibly once a probe reorientation measurement starts and ends in the post-yield regime.

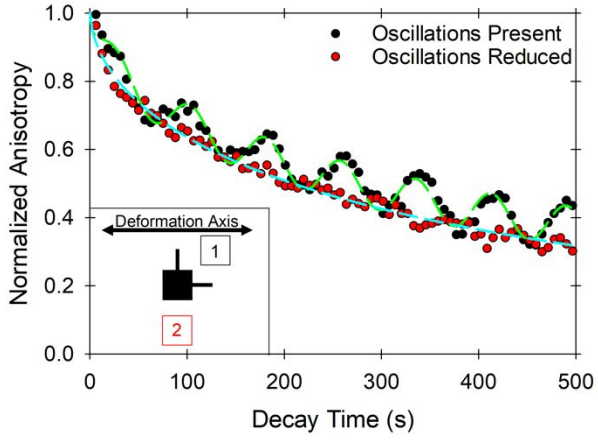

Figure 2. Comparison of anisotropy decay with and without large oscillations from strain-induced birefringence, controlled as explained in the text. The oscillating decay is captured by the sum of a stretched exponential and a sinusoid. The stretched exponential parameters for the oscillating and non-oscillating decays shown are $\log\left(\tau_{KWW}/s\right) = 2.70$, $\beta_{KWW} = 0.561$ and $\log\left(\tau_{KWW}/s\right) = 2.60$, $\beta_{KWW} = 0.577$, respectively. The inset is a schematic showing the position of photobleaching measurements (black pattern) and reference measurements that lead to anisotropy oscillations (1) and that do not lead to anisotropy oscillations (2).

While previous measurements of the anisotropy decay during the deformation of PMMA glasses showed a smooth decay, some measurements performed on PLA glasses during deformation showed a clear oscillatory behavior on top of the smooth decay. As explained below, we understand the origin of the oscillations and they do not affect our measurement of the segmental dynamics of the system. Figure 2 shows two anisotropy measurements gathered one after the other in the post-yield regime on the same sample; in this regime, the same segmental relaxation time is expected for both measurements. The oscillating anisotropy decay can be fit with the sum of a KWW function and a sinusoidal term as shown in Figure 2. Comparing the

KWW parameters of the oscillating and smooth anisotropy decays shows that the oscillations do not affect our ability to extract an accurate τ_{KWW} and β_{KWW}.

The oscillatory anisotropy decay shown in Figure 2 is due to a combination of Fabry-Perot interference (induced by a change in thickness during deformation) and a position-dependent, deformation-induced birefringence. Briefly, the changing thickness during deformation causes oscillations in the probe beam intensity inside the sample, leading to oscillations in the two orthogonally polarized fluorescence channels. The oscillations in the two fluorescence channels then become out-of-phase between the photobleached location and the reference location due to deformation-induced birefringence that varies along the deformation axis. We found that oscillations occurred in experiments where the reference intensities were displaced along the deformation axis from the photobleached location (box 1 in Figure 2 inset), while the oscillations were minimized when the reference intensities were measured in the same position along the deformation axis (box 2 in Figure 2 inset). Though we have seen oscillations in the polarized fluorescence intensities during previous measurements on PMMA during deformation, we have not seen oscillations in the anisotropy. Simple optical microscopy observations (not shown here) suggest that PLA has a larger birefringence than PMMA at the same post-yield strain value, which is consistent with the magnitude of reported stress-optical coefficients of molten PLA and PMMA (3.1 GPa^{-1} and 0.15 GPa^{-1}, respectively[47-49]). Thus, it is reasonable that anisotropy oscillations are observed in PLA but not PMMA. This explanation for the oscillations is also consistent with the observation that the frequency and amplitude of the fluorescence intensity oscillations is dependent on the local strain rate and the sample thickness, respectively. As a check on our understanding, we verified that the observed oscillations, in

combination with a model of Fabry-Perot interference with corrections for a diverging light source, can accurately predict the local strain rate and thickness of the sample (not shown).

Results

Segmental Dynamics of Quiescent PLA. Although the main focus of this work is the effect of constant strain rate deformation on the segmental dynamics of glassy PLA, it is important to establish that the probe reorientation technique can accurately describe the segmental dynamics of the quiescent system. Probe reorientation measurements were performed on quiescent PLA at various temperatures below T_g to generate anisotropy decays like those shown in Figure 3.

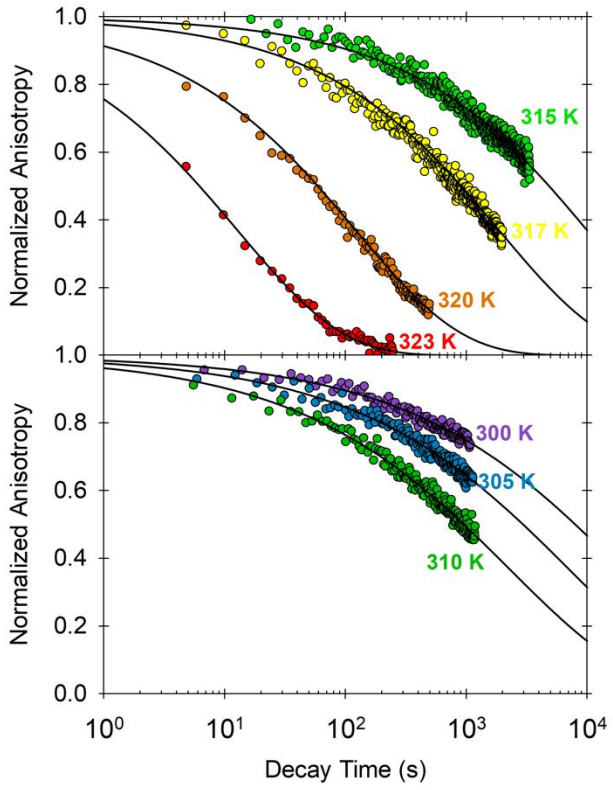

Figure 3. Anisotropy decays measured in quiescent PLA at various temperatures below $T_{g,DSC}$ = 325 K. Filled circles are data points, and the solid lines are fits to a KWW function. Upper: Dynamics after isothermal aging to equilibrium. Lower: Dynamics after isothermal aging for 30 minutes.

The upper panel shows representative anisotropy decays for PLA that has been aged to equilibrium at temperatures between 315 K and 323 K (T_g – 10 K to T_g – 2 K). These measurements were tracked over the course of 48 hours and were considered to be in equilibrium

when the anisotropy decay was found to be unchanging over the course of 24 hours. The anisotropy for these equilibrium systems are well described by a KWW function with $\beta_{KWW} = 0.50$. This is consistent with the range 0.46-0.53 from experiment[50, 51] and simulation[52], as well as the value 0.49 obtained from our own analysis of dynamic mechanical data[53] that displays the same dynamics as our system, as described below. The lower panel of Figure 3 shows anisotropy decays for glassy PLA between 300 K and 310 K (T_g – 25 K to T_g – 15 K), temperatures also used for constant strain rate deformations. This data was gathered after isothermal aging for 30 minutes and is well described by a KWW function with $\beta_{KWW} = 0.42$. The β_{KWW} parameter for all KWW fits on quiescent PLA were constrained to 0.50 and 0.42 (for equilibrium data and aging data, respectively) to reduce the error in the estimate of the relaxation time. A plot similar to Figure 3 that includes the response for PLA at 317 K and 315 K after isothermal aging for 30 minutes can be found in the supporting information (Figure S2).

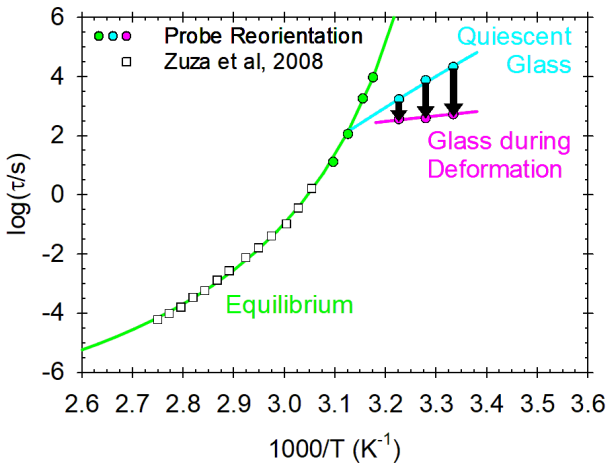

Figure 4. Relaxation times for PLA melts and glasses. The open squares are DMA data points extracted from Zuza et al. [53], shifted upward by 0.87 decades, and the filled circles are probe reorientation times measured in the present work at equilibrium, in the quiescent glass, and in the flow regime during isothermal deformation of the glass. The arrows represent the range of relaxation times measured during deformation while the pink line is representative of a single local strain rate, $\dot{\varepsilon}_{local} = 10^{-4}$ s^{-1}.

Figure 4 shows that the equilibrium relaxation times extracted from probe reorientation measurements in PLA (green data points) have the same temperature dependence as reported relaxation times of PLA measured from dynamic mechanical analysis;[53] the PLA from ref [53] has a high molecular weight ($M_v = 3.8 \times 10^5$ g/mol) and an L/D ratio of 50/50, similar to the

PLA studied here. The DMA data have been shifted vertically upward by 0.87 decades to align with the equilibrium probe reorientation measurements. Equilibrium relaxation times of supercooled liquids are commonly described by the empirical Vogel-Fulcher-Tammann (VFT) equation:

$$\log\left(\tau(T)/s\right) = A + \frac{B}{T - T_0}$$

Fitting the DMA data and the equilibrium probe reorientation times with the VFT equation yields $A = -9.4, B = 421\ K, T_0 = 283\ K$, shown by the green line in Figure 4.

As expected, the relaxation times of the PLA glasses do not fall on the equilibrium line, but instead have a more Arrhenius-like temperature dependence, as shown by the blue data points in Figure 4. Also shown in Figure 4 are relaxation times measured during deformation, indicated by the pink data points and black arrows. We will return to these in the discussion section.

Segmental Dynamics of PLA Glasses during Deformation. The main results of this work focus on the segmental dynamics of glassy PLA during constant strain rate deformation. Typical stress-strain curves for PLA glasses deformed with a global strain rate $\dot{\varepsilon} = 3.1 \times 10^{-5}$ s^{-1} at different temperatures are shown in Figure 5.

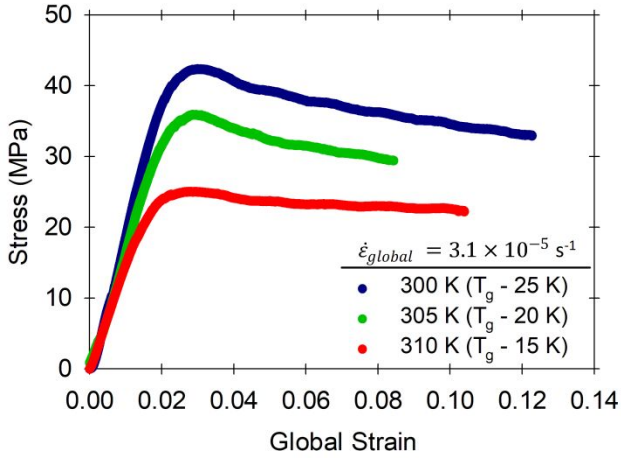

Figure 5. Typical stress-strain curves for glassy PLA during constant strain rate tensile deformation.

These curves show the expected features of deforming polymer glasses: at low strains (less than 0.01), the stress rises linearly with increasing strain; at higher strains, the stress begins to turn over and reaches a local maximum at the yield stress (the yield strain is 0.03); beyond yield, the stress slowly decreases and approaches the flow stress. In the experiments reported below, deformations were limited to global strains below 0.15 to minimize failure of the samples while allowing for sufficient time in the post-yield regime to perform multiple probe reorientation measurements. Because of this, the strain hardening regime is not explored in these measurements. The elastic modulus for the deformations range between 1950 MPa at the lowest temperature to 1500 MPa at the highest temperature. These values fall within the range of values reported in the literature,[45, 54-56] though the method of preparation, thermal history and stereochemical composition can modify the mechanical properties of PLA (with reported modulus values from 700 MPa to 4000 MPa). Other features of the curves in Figure 5, like the increase of the yield stress and flow stress with decreasing temperature, are typical thermo-mechanical signatures of polymer glasses.[2]

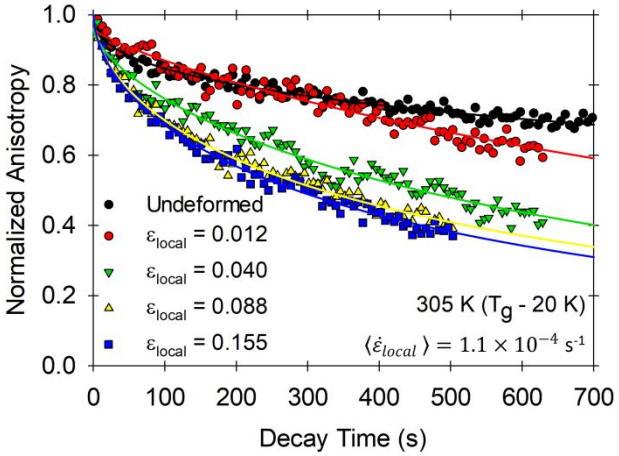

Figure 6. Typical normalized anisotropy decays gathered at increasing strain during constant strain rate deformation, indicating faster dynamics with increasing strain.

Probe reorientation measurements were performed before and during deformation to track changes in the segmental dynamics. As seen by the changes in the anisotropy curves shown in Figure 6, segmental dynamics can be accelerated during a constant strain rate deformation.

Figure 6 shows anisotropy curves collected at various local strains during a constant strain rate deformation at T_g – 20 K with an average post-yield strain rate $\langle \dot{\varepsilon}_{local} \rangle = 1.1 \times 10^{-4}$ s^{-1}. Also shown are KWW fits to each anisotropy curve. The deformation conditions for this experiment caused the anisotropy to decay faster as the deformation proceeds, until strains well past the yield strain are reached. At this point, the anisotropy decays at the same rate, within experimental error. Quantitative characterization of the decay rate and shape by the values of τ_{KWW} and β_{KWW}, respectively, illuminate how constant strain rate deformation affects the segmental dynamics of PLA during deformation.

Collections of anisotropy decays, like those shown in Figure 6, were obtained from glassy PLA samples held at various temperatures and deformed at various strain rates. Relaxation times extracted from these anisotropy decays are plotted as a function of strain in Figure 7 to show the evolution of the segmental dynamics during deformation. In both the upper and lower plots, the average relaxation time for the undeformed polymer at each temperature is indicated by colored arrows. The data is grouped and labelled by the average local strain rate, calculated as the average value of local strain rates measured in the post-yield regime for each experiment in the group.

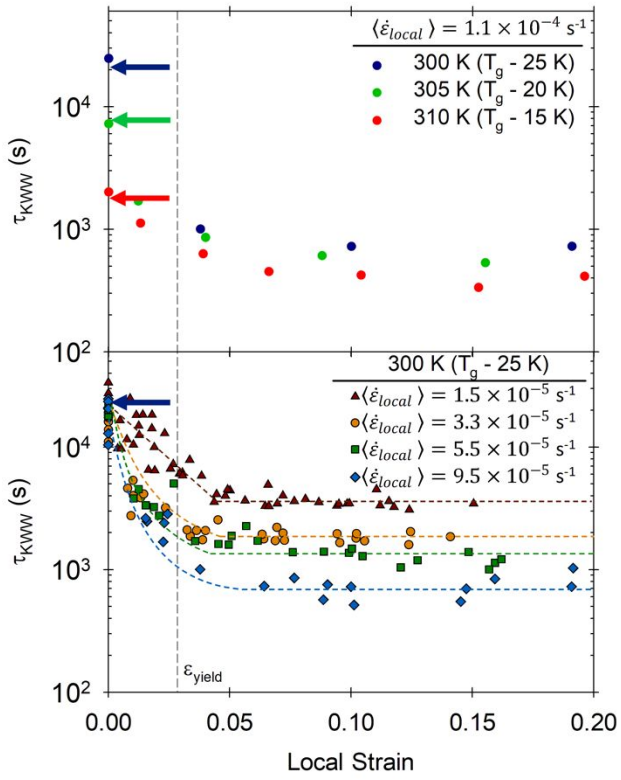

Figure 7. Evolution of segmental relaxation time during constant strain rate deformation. The colored arrows represent the average relaxation time for the undeformed system at the specified temperature. The vertical black line (dashed) shows the yield strain. Local strain rates are averages in the post-yield regime. Upper: Deformation at three different temperatures with the same local strain rate. Lower: Deformation at 300 K with four different local strain rates. Dashed curves are guides to the eye.

The upper plot in Figure 7 shows how τ_{KWW} changes during deformations that occur at different temperatures, all with the same post-yield local strain rate, $\langle\dot{\varepsilon}_{local}\rangle = 1.1 \times 10^{-4}$ s^{-1}. The lower plot shows the changes for τ_{KWW} during deformations at a single temperature (T_g – 25 K) with various post-yield local strain rates. For all of the conditions shown, the segmental relaxation times decreases from the undeformed relaxation time until strains beyond the yield strain (represented by the black dashed line), when a plateau value is reached. A similar plot for the evolution of β_{KWW} during deformation is shown in the supplemental material (Figure S3). The change in the dynamics due to deformation depends on both the temperature and local strain rate; at a single local strain rate this change spans from a factor of 30 at T_g – 25 K to a factor of 4 at T_g – 15 K, while at a single temperature it spans from a factor of 30 at $\langle\dot{\varepsilon}_{local}\rangle = 9.5 \times 10^{-5}$ s^{-1} to a factor of 5 at $\langle\dot{\varepsilon}_{local}\rangle = 1.5 \times 10^{-5}$ s^{-1}. To better understand the relationship between

temperature, local strain rate and segmental dynamics in glassy PLA, we will focus on measurements in the post-yield regime where the segmental relaxation times are nearly constant.

Figure 8 shows a strong correlation between the segmental relaxation time of glassy PLA in the post-yield regime and the local strain rate for all temperatures investigated here. Each data point in Figure 8 represents a single probe reorientation time and local strain rate measurement. The strong correlation shown in Figure 8 is well-described by a power-law relationship, illustrated by the colored dashed lines. The slopes of the best-fit lines (with the standard error of the estimate) are -0.85 ± 0.02, -0.82 ± 0.04, and -0.77 ± 0.02 from top to bottom. This dependence of the relaxation time on the strain rate indicates that PLA glasses respond qualitatively like a shear-thinning fluid (with $\tau_{KWW} \propto \eta_{apparent} \propto \dot{\varepsilon}^{n-1}, n < 1$) in the post-yield regime of the deformation.

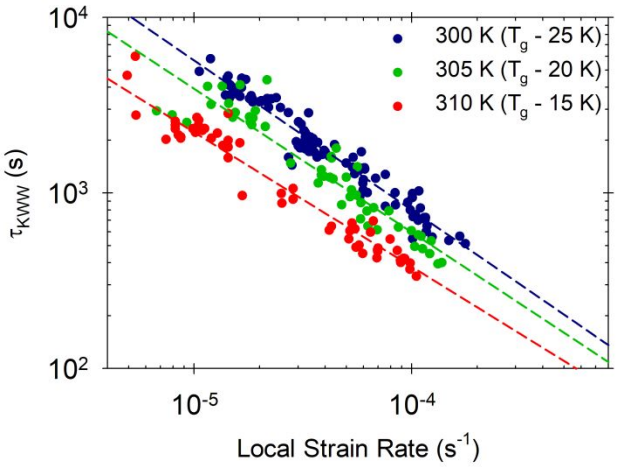

Figure 8. Relaxation times versus local strain rate for measurements in the post-yield regime. The dashed lines are power-law fits to the data. Slopes of the lines, from top to bottom, are: -0.85 (±0.02), -0.82 (±0.04), and -0.77 (±0.02).

Discussion

Figure 4 provides a useful overview of the results presented here on segmental dynamics in PLA glasses. The figure shows data collected for the quiescent glass (blue data points) and data collected for the glass during deformation at the highest strain rate in the post-yield regime (pink data points). The relaxation times measured during deformation across the three temperatures explored here are much closer to each other than the relaxation times of the

quiescent glasses across the same temperature range. Indeed, the temperature dependence of the dynamics during deformation are about 32 K/decade, compared to about 9 K/decade for the dynamics of the quiescent glasses, both of which are much weaker than the observed temperature dependence of the equilibrium dynamics near T_g. On the other hand, the slopes described in Figure 7 indicate that changing the strain rate of a deformation by only a factor of 2.5 would cause the same change in relaxation times as changing the temperature by 10 K. Together, these results show that the strain rate of the deformation is the dominant factor in determining the segmental dynamics. Though temperature still has an effect on segmental dynamics during deformation, its role is greatly reduced compared to the equilibrium melt and even to the quiescent glass.

In the following discussion, we will compare the effects of constant strain rate deformation on the segmental dynamics of PLA glasses to those of lightly crosslinked PMMA glasses. In particular, we will show that the changes of the segmental relaxation times and the dynamic heterogeneity of these two polymer glasses are very similar. This argues that observed features represent the generic response of polymer glasses to constant strain rate deformation.

Comparison of τ_{KWW}. The data in Figure 8 allows for a simple, direct comparison between the combined effects of temperature and strain rate on the post-yield relaxation times in glasses of PLA and lightly crosslinked PMMA. This comparison is shown in the upper panel of Figure 9, which combines the PLA data from Figure 8 with the solid lines showing fits to data on lightly crosslinked PMMA from ref [40]. Comparing the two polymers, the exponents of power-law fits (the slope of the lines) are the same (to within 0.1) at the same temperature relative to T_g, and for both polymers they appear to approach -1 as the temperature is decreased. The similarity of these responses is made more apparent in the lower panel of Figure 9. Here the absolute

values of τ_{KWW} for PLA glasses have be shifted downward by a factor of three to emphasize the similarity to the PMMA data for any given temperature relative to T_g. We emphasize that the power-law relationships shown in Figure 9 are effectively the same for the two polymers, despite the existence of an overlapping secondary relaxation in PMMA.[43, 44] The similarity of the exponents for the two systems as a function of temperature indicate that these are robust features of polymer glass deformation. The values for these exponents are near the value of -0.8 reported for colloidal glasses,[57, 58] and they are consistent with simulations of bead-spring polymers.[26, 27] NLE theory predicts similar values for these exponents in polymer glasses[17] and colloidal glasses.[59] The weak temperature dependence of the exponents can also be explained in the context of NLE theory.[17]

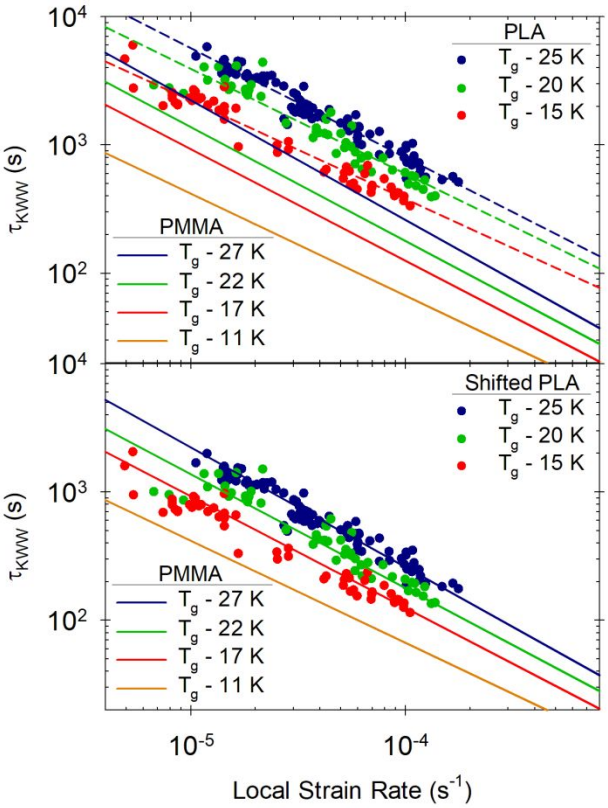

Figure 9. Upper: Relaxation times in the post-yield regime versus local strain rate for PLA (filled circles and dashed lines) and PMMA (solid lines – fit to PMMA data from ref [40]). PLA and PMMA relaxation times show very similar behavior in the post-yield regime. Lower: PLA data shifted downward by a factor of 3 to emphasize the similarity in the behavior.

The lower panel of Figure 9 indicates that the absolute values of τ_{KWW} for PLA glasses are roughly three times longer than those observed for PMMA glasses for any given temperature

and strain rate. The same factor of three has also been observed in the probe reorientation time scale in the two glasses measured during physical aging.[46,60] In these experiments, the relaxation time of PLA[60] and PMMA[46] glasses are measured during physical aging through stress relaxation after a linear step strain deformation and with probe reorientation in the absence of deformation. When the two systems show the same mechanical relaxation time, the probe reorientation time scale for PLA is 0.5 decades longer than the probe reorientation time scale for PMMA, similar to the difference seen here. We attribute the difference in the probe reorientation time scale to the size of the probe relative to chain segments in each polymer system, i.e., the length scale of structural relaxation near T_g in PLA is smaller in absolute terms than the corresponding length scale for PMMA. In the absence of other interactions, it has been shown that increasing probe size for a given host polymer increases the probe reorientation time.[61-63]

Comparison of β_{KWW}. Along with the characteristic relaxation time τ_{KWW}, the dynamic heterogeneity of PLA, indicated by the value of β_{KWW}, is tracked during deformation. In Figure 10, the values of β_{KWW} in the post-yield regime obtained from PLA are compared to those obtained from PMMA in ref [40].

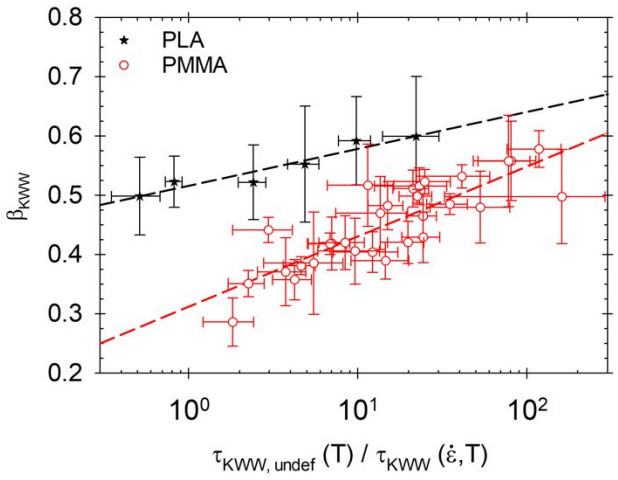

Figure 10. Values of the β parameter from the KWW fit to anisotropy data collected in the post-yield regime. The x-axis is a measure of the acceleration in dynamics compared to the initial undeformed system. Filled stars represent measurements on PLA and open circles represent measurements on PMMA (from ref [40]). Error bars represent one standard deviation. Dashed lines show linear fits through each data set.

β_{KWW} for PLA increases from a value of 0.42 in the undeformed state to about 0.60 for the largest deformation-induced increases in segmental mobility, while β_{KWW} for PMMA increases from 0.31 in the undeformed state to about 0.57. The increases in β_{KWW} during the deformation of PMMA glasses have been interpreted previously as a narrowing of the distribution of relaxation times.[37, 39] Thus for both PLA and PMMA, the more deformation decreases relaxation times (faster segmental dynamics), the more it narrows the original distribution of relaxation times. By representing the KWW function as a series of weighted exponentials,[64] the distribution of relaxation times for specific β_{KWW} can be constructed. This method indicates that the FWHM of the distribution of relaxation times for PLA decreases from 2.1 decades to 1.1 decades during deformation while that of PMMA decreases from 3.1 decades to 1.2 decades, a significant narrowing for both systems. While experiments have shown that crosslinking can affect the heterogeneity of the underlying dynamics in a PMMA glass,[41] the changes in β_{KWW} with deformation seen in both PLA and PMMA glasses suggest that a narrowing of the distribution of relaxation times is a generic feature of polymer glass deformation.

A narrowing of the distribution of relaxation times due to deformation is predicted by the stochastic constitutive model of Medvedev and Caruthers.[20] The model incorporates material properties of a polymer glass to develop a fully tensorial, mesoscale description of the macroscopic response to deformation. An important feature of the model is the natural occurrence of a distribution of relaxation times, which is also seen to evolve during deformation. In particular, the model predicts that the distribution of relaxation times for a lightly crosslinked PMMA glass shifts to faster times and narrows as deformation proceeds into the flow regime during uniaxial tensile deformation.[65] In ref [65], the FWHM of the distribution narrows from 4 decades to 2.4 decades during deformation with a strain rate $\dot{\varepsilon} = 10^{-4}$ s^{-1}. The change in FWHM

agrees reasonably with the narrowing in PMMA described above. Furthermore, we fit the relaxation time distributions to a KWW distribution to extract τ_{KWW} and β_{KWW}, which we then analyzed to determine the relationship between β_{KWW} and the acceleration from the undeformed system. This analysis (not shown here) of PMMA results from ref [65] shows an average increase of 0.10 in β_{KWW} for each decade of acceleration in the average relaxation time, consistent with the value of 0.12 increase per decade observed experimentally for PMMA. The agreement shown between the model and experiments for PMMA supports the mechanism that causes narrowing in the model. The new data for PLA presented here could be used to further test this mechanism.

A coarse-grained model by Conca et al.[23] has qualitatively reproduced changes in segmental dynamics of a polymer glass during constant strain rate deformation. This model relies on a facilitation mechanism to allow fast and slow mesoscopic subunits to relax during deformation. It also includes a distribution of relaxation times which evolves as the mesoscopic subunits relax. Full knowledge of the distribution of relaxation times at any given time during deformation allows for the authors to create a macroscopic relaxation function which can then be fit to a KWW function to mimic the analysis done on probe reorientation measurements. The β_{KWW} parameter from the model shows a qualitative similarity to experiments on lightly crosslinked PMMA, with β_{KWW} increasing from the undeformed state to the plastic flow regime. As with the SCM above, we have analyzed the data provided in ref [23] to determine the relationship between β_{KWW} and acceleration from the undeformed system. This analysis shows an average increase of 0.24 in β_{KWW} for each decade of acceleration, nearly double what is observed experimentally in PMMA. It is possible that choosing alternate model parameters will

allow for a more quantitative description of the experimental results for PMMA, and also allow a description of the experimental results from PLA displayed here.

Conclusion

Here we have shown that the segmental dynamics of poly(lactic acid) glasses and lightly crosslinked poly(methyl methacrylate) glasses show the same generic behavior during constant strain rate deformation, as measured using the probe reorientation technique. The changes in the characteristic relaxation time of PLA glasses during plastic flow were shown to strongly depend on the local strain rate via a power-law relationship, with a weakly temperature-dependent exponent, which parallels previous results from lightly crosslinked PMMA. The temperature dependence of the relaxation time in the plastic flow regime was also shown to be the same for PLA and PMMA glasses. The distribution of relaxation times of PLA glasses was also shown to narrow during deformation, again like PMMA. The similarities reported here in the two polymer glass systems suggest that these effects are the generic consequences of constant strain rate deformation on the segmental dynamics of polymer glasses. Though some models are able to qualitatively describe the segmental dynamics of PMMA during constant strain rate deformation, this new work is anticipated to allow for further refinement of these models for a closer quantitative description. This would allow for a more complete understanding of the microscopic details of the deformation of polymer glasses and, in turn, better prediction of the mechanical and engineering properties of polymer glasses.

Acknowledgements

We thank the National Science Foundation (DMR-1708248) for support of this work. We thank Enran Xing for helpful discussions.

References

1. McKenna, G. B.; Simon, S. L. 50th Anniversary Perspective: Challenges in the Dynamics and Kinetics of Glass-Forming Polymers. *Macromolecules* **2017,** 50 (17), 6333-6361 DOI: 10.1021/acs.macromol.7b01014.

2. Caruthers, J. M.; Medvedev, G. A., Thermo-Mechanical Signatures of Polymeric Glasses. In *Polymer Glasses*, First ed.; Roth, C. B., Ed. CRC Press: 2016.

3. Ediger, M. D. Spatially heterogeneous dynamics in supercooled liquids. *Annu Rev Phys Chem* **2000,** 51, 99-128 DOI: 10.1146/annurev.physchem.51.1.99.

4. Richert, R. Heterogeneous dynamics in liquids: fluctuations in space and time. *J Phys-Condens Mat* **2002,** 14 (23), R703-R738 DOI: 10.1088/0953-8984/14/23/201.

5. Rottler, J.; Schoenholz, S. S.; Liu, A. J. Predicting plasticity with soft vibrational modes: from dislocations to glasses. *Phys Rev E Stat Nonlin Soft Matter Phys* **2014,** 89 (4), 042304 DOI: 10.1103/PhysRevE.89.042304.

6. Berthier, L.; Ediger, M. D. Facets of Glass Physics. *Phys Today* **2016,** 69 (1), 40-46 DOI: 10.1063/Pt.3.3052.

7. Hoy, R. S.; Robbins, M. O. Strain hardening of polymer glasses: entanglements, energetics, and plasticity. *Phys Rev E Stat Nonlin Soft Matter Phys* **2008,** 77 (3 Pt 1), 031801 DOI: 10.1103/PhysRevE.77.031801.

8. Liu, Z. N.; Li, X. X.; Zheng, Y. X.; Wang, S. Q.; Tsige, M. Chain Network: Key to the Ductile Behavior of Polymer Glasses. *Macromolecules* **2018,** 51 (5), 1666-1673 DOI: 10.1021/acs.macromol.7b01764.

9. Wang, S. Q.; Cheng, S.; Lin, P.; Li, X. A phenomenological molecular model for yielding and brittle-ductile transition of polymer glasses. *J Chem Phys* **2014,** 141 (9), 094905 DOI: 10.1063/1.4893765.

10. Cubuk, E. D.; Ivancic, R. J. S.; Schoenholz, S. S.; Strickland, D. J.; Basu, A.; Davidson, Z. S.; Fontaine, J.; Hor, J. L.; Huang, Y. R.; Jiang, Y.; Keim, N. C.; Koshigan, K. D.; Lefever, J. A.; Liu, T.; Ma, X. G.; Magagnosc, D. J.; Morrow, E.; Ortiz, C. P.; Rieser, J. M.; Shavit, A.; Still, T.; Xu, Y.; Zhang, Y.; Nordstrom, K. N.; Arratia, P. E.; Carpick, R. W.; Durian, D. J.; Fakhraai, Z.; Jerolmack, D. J.; Lee, D.; Li, J.; Riggleman, R.; Turner, K. T.; Yodh, A. G.; Gianola, D. S.; Liu, A. J. Structure-property relationships from universal signatures of plasticity in disordered solids. *Science* **2017,** 358 (6366), 1033-1037 DOI: 10.1126/science.aai8830.

11. Argon, A. S. Plastic Deformation in Metallic Glasses. *Acta Metallurgica* **1979,** 27 (1), 47-58 DOI: 10.1016/0001-6160(79)90055-5.

12. Eyring, H. Viscosity, plasticity, and diffusion as examples of absolute reaction rates. *Journal of Chemical Physics* **1936,** 4 (4), 283-291 DOI: 10.1063/1.1749836.

13. Fielding, S. M.; Larson, R. G.; Cates, M. E. Simple model for the deformation-induced relaxation of glassy polymers. *Phys Rev Lett* **2012,** 108 (4), 048301 DOI: 10.1103/PhysRevLett.108.048301.

14. Fielding, S. M.; Moorcroft, R. L.; Larson, R. G.; Cates, M. E. Modeling the relaxation of polymer glasses under shear and elongational loads. *J Chem Phys* **2013,** 138 (12), 12A504 DOI: 10.1063/1.4769253.

15. Zou, W.; Larson, R. G. A hybrid Brownian dynamics/constitutive model for yielding, aging, and rejuvenation in deforming polymeric glasses. *Soft Matter* **2016,** 12 (32), 6757-70 DOI: 10.1039/c6sm00851h.

16. Klompen, E. T. J.; Engels, T. A. P.; Govaert, L. E.; Meijer, H. E. H. Modeling of the postyield response of glassy polymers: Influence of thermomechanical history. *Macromolecules* **2005,** 38 (16), 6997-7008 DOI: 10.1021/ma050498v.

17. Chen, K.; Schweizer, K. S. Theory of Yielding, Strain Softening, and Steady Plastic Flow in Polymer Glasses under Constant Strain Rate Deformation. *Macromolecules* **2011,** 44 (10), 3988-4000 DOI: 10.1021/ma200436w.

18. Chen, K.; Schweizer, K. S. Theory of physical aging in polymer glasses. *Phys Rev E Stat Nonlin Soft Matter Phys* **2008,** 78 (3 Pt 1), 031802 DOI: 10.1103/PhysRevE.78.031802.

19. Chen, K.; Schweizer, K. S. Theory of aging, rejuvenation, and the nonequilibrium steady state in deformed polymer glasses. *Phys Rev E Stat Nonlin Soft Matter Phys* **2010,** 82 (4 Pt 1), 041804 DOI: 10.1103/PhysRevE.82.041804.

20. Medvedev, G. A.; Caruthers, J. M. Development of a stochastic constitutive model for prediction of postyield softening in glassy polymers. *J Rheol* **2013,** 57 (3), 949-1002 DOI: 10.1122/1.4801958.

21. Merabia, S.; Long, D. Heterogeneous dynamics, ageing, and rejuvenating in van der Waals liquids. *J Chem Phys* **2006,** 125 (23), 234901 DOI: 10.1063/1.2399527.

22. Dequidt, A.; Conca, L.; Delannoy, J. Y.; Sotta, P.; Lequeux, F.; Long, D. R. Heterogeneous Dynamics and Polymer Plasticity. *Macromolecules* **2016,** 49 (23), 9148-9162 DOI: 10.1021/acs.macromol.6b01375.

23. Conca, L.; Dequidt, A.; Sotta, P.; Long, D. R. Acceleration and Homogenization of the Dynamics during Plastic Deformation. *Macromolecules* **2017,** 50 (23), 9456-9472 DOI: 10.1021/acs.macromol.7b01391.

24. Warren, M.; Rottler, J. Deformation-induced accelerated dynamics in polymer glasses. *J Chem Phys* **2010,** 133 (16), 164513 DOI: 10.1063/1.3505149.

25. Riggleman, R. A.; Schweizer, K. S.; de Pablo, J. J. Nonlinear creep in a polymer glass. *Macromolecules* **2008,** 41 (13), 4969-4977 DOI: 10.1021/ma8001214.

26. Riggleman, R. A.; Toepperwein, G. N.; Papakonstantopoulos, G. J.; de Pablo, J. J. Dynamics of a glassy polymer composite during active deformation. *Macromolecules* **2009,** 42 (10), 3632-3640.

27. Rottler, J. Molecular mobility in driven monomeric and polymeric glasses. *Phys Rev E* **2018,** 98 (1-1), 010501 DOI: 10.1103/PhysRevE.98.010501.

28. Rottler, J. Relaxation times in deformed polymer glasses: A comparison between molecular simulations and two theories. *Journal of Chemical Physics* **2016,** 145 (6), 064505 DOI: 10.1063/1.4960208.

29. Yee, A. F.; Bankert, R. J.; Ngai, K. L.; Rendell, R. W. Strain and Temperature Accelerated Relaxation in Polycarbonate. *J Polym Sci Pol Phys* **1988,** 26 (12), 2463-2483 DOI: 10.1002/polb.1988.090261206.

30. Martinez-Vega, J. J.; Trumel, H.; Gacougnolle, J. L. Plastic deformation and physical ageing in PMMA. *Polymer* **2002,** 43 (18), 4979-4987 DOI: 10.1016/S0032-3861(02)00332-4.

31. Mckenna, G. B.; Zapas, L. J. Superposition of Small Strains on Large Deformations as a Probe of Nonlinear Response in Polymers. *Polym Eng Sci* **1986,** 26 (11), 725-729 DOI: 10.1002/pen.760261103.

32. Loo, L. S.; Cohen, R. E.; Gleason, K. K. Chain mobility in the amorphous region of nylon 6 observed under active uniaxial deformation. *Science* **2000,** 288 (5463), 116-9.

33. Zhou, Q. Y.; Argon, A. S.; Cohen, R. E. Enhanced Case-II diffusion of diluents into glassy polymers undergoing plastic flow. *Polymer* **2001,** 42 (2), 613-621 DOI: 10.1016/S0032-3861(00)00376-1.

34. Kalfus, J.; Detwiler, A.; Lesser, A. J. Probing Segmental Dynamics of Polymer Glasses during Tensile Deformation with Dielectric Spectroscopy. *Macromolecules* **2012,** 45 (11), 4839-4847 DOI: 10.1021/ma202708j.

35. Perez-Aparicio, R.; Cottinet, D.; Crauste-Thibierge, C.; Vanel, L.; Sotta, P.; Delannoy, J. Y.; Long, D. R.; Ciliberto, S. Dielectric Spectroscopy of a Stretched Polymer Glass: Heterogeneous Dynamics and Plasticity. *Macromolecules* **2016,** 49 (10), 3889-3898 DOI: 10.1021/acs.macromol.5b02635.

36. Lee, H. N.; Paeng, K.; Swallen, S. F.; Ediger, M. D. Direct measurement of molecular mobility in actively deformed polymer glasses. *Science* **2009,** 323 (5911), 231-4 DOI: 10.1126/science.1165995.

37. Lee, H. N.; Paeng, K.; Swallen, S. F.; Ediger, M. D.; Stamm, R. A.; Medvedev, G. A.; Caruthers, J. M. Molecular Mobility of Poly(methyl methacrylate) Glass During Uniaxial Tensile Creep Deformation. *J Polym Sci Pol Phys* **2009,** 47 (17), 1713-1727 DOI: 10.1002/polb.21774.

38. Lee, H. N.; Riggleman, R. A.; de Pablo, J. J.; Ediger, M. D. Deformation-Induced Mobility in Polymer Glasses during Multistep Creep Experiments and Simulations. *Macromolecules* **2009,** 42 (12), 4328-4336 DOI: 10.1021/ma900394n.

39. Bending, B.; Christison, K.; Ricci, J.; Ediger, M. D. Measurement of Segmental Mobility during Constant Strain Rate Deformation of a Poly(methyl methacrylate) Glass. *Macromolecules* **2014,** 47 (2), 800-806 DOI: 10.1021/ma402275r.

40. Hebert, K.; Bending, B.; Ricci, J.; Ediger, M. D. Effect of Temperature on Postyield Segmental Dynamics of Poly(methyl methacrylate) Glasses: Thermally Activated Transitions Are Important. *Macromolecules* **2015,** 48 (18), 6736-6744 DOI: 10.1021/acs.macromol.5b01486.

41. Alves, N. M.; Ribelles, J. L. G.; Gomez-Tejedor, J. A.; Mano, J. F. Viscoelastic behavior of poly(methyl methacrylate) networks with different cross-linking degrees. *Macromolecules* **2004,** 37 (10), 3735-3744 DOI: 10.1021/ma035626z.

42. Shen, J. X.; Lin, X. S.; Liu, J.; Li, X. Effects of Cross-Link Density and Distribution on Static and Dynamic Properties of Chemically Cross-Linked Polymers. *Macromolecules* **2019,** 52 (1), 121-134 DOI: 10.1021/acs.macromol.8b01389.

43. Fytas, G.; Wang, C. H.; Fischer, E. W.; Mehler, K. Evidence of two relaxation processes in the photon correlation spectra of poly(methyl methacrylate) above Tg. *J Polym Sci Pol Phys* **1986,** 24 (8), 1859-1867.

44. Bergman, R.; Alvarez, F.; Alegria, A.; Colmenero, J. The merging of the dielectric α- and β-relaxations in poly(methyl methacrylate). *Journal of Chemical Physics* **1998,** 109 (17), 7546-7555 DOI: 10.1063/1.477376.

45. Huang, T.; Miura, M.; Nobukawa, S.; Yamaguchi, M. Chain Packing and Its Anomalous Effect on Mechanical Toughness for Poly(lactic acid). *Biomacromolecules* **2015,** 16 (5), 1660-6 DOI: 10.1021/acs.biomac.5b00293.

46. Ricci, J.; Bennin, T.; Ediger, M. D. Direct Comparison of Probe Reorientation and Linear Mechanical Measurements of Segmental Dynamics in Glassy Poly(methyl methacrylate). *Macromolecules* **2018,** 51 (19), 7785-7793 DOI: 10.1021/acs.macromol.8b01522.

47. Mulligan, J.; Cakmak, M. Nonlinear mechanooptical behavior of uniaxially stretched poly(lactic acid): Dynamic phase behavior. *Macromolecules* **2005,** 38 (6), 2333-2344 DOI: 10.1021/ma048794f.

48. Kahar, N.; Duckett, R. A.; Ward, I. M. Stress Optical Studies of Oriented Poly(Methyl Methacrylate). *Polymer* **1978,** 19 (2), 136-144 DOI: 10.1016/0032-3861(78)90029-0.

49. Marrucci, G.; de Cindio, B. The stress relaxation of molten PMMA at large deformations and its theoretical interpretation. *Rheologica Acta* **1980,** 19 (1), 68-75.

50. Mierzwa, M.; Floudas, G.; Dorgan, J.; Knauss, D.; Wegner, J. Local and global dynamics of polylactides. A dielectric spectroscopy study. *J Non-Cryst Solids* **2002,** 307, 296-303 DOI: 10.1016/S0022-3093(02)01480-1.

51. Mijovic, J.; Sy, J. W. Molecular dynamics during crystallization of poly(L-lactic acid) as studied by broad-band dielectric relaxation spectroscopy. *Macromolecules* **2002,** 35 (16), 6370-6376 DOI: 10.1021/ma0203647.

52. Xiang, T. X.; Anderson, B. D. Water uptake, distribution, and mobility in amorphous poly(D,L-lactide) by molecular dynamics simulation. *J Pharm Sci* **2014,** 103 (9), 2759-2771 DOI: 10.1002/jps.23855.

53. Zuza, E.; Ugartemendia, J. M.; Lopez, A.; Meaurio, E.; Lejardi, A.; Sarasua, J. R. Glass transition behavior and dynamic fragility in polylactides containing mobile and rigid amorphous fractions. *Polymer* **2008,** 49 (20), 4427-4432 DOI: 10.1016/j.polymer.2008.08.012.

54. Pluta, M.; Galeski, A. Plastic deformation of amorphous poly(L/DL-lactide): structure evolution and physical properties. *Biomacromolecules* **2007,** 8 (6), 1836-43 DOI: 10.1021/bm061229v.

55. Camarero-Espinosa, S.; Boday, D. J.; Weder, C.; Foster, E. J. Cellulose Nanocrystal Driven Crystallization of Poly(D,L-lactide) and Improvement of the Thermomechanical Properties. *J Appl Polym Sci* **2015,** 132 (10), DOI: 10.1002/app.41607.

56. Perego, G.; Cella, G. D.; Bastioli, C. Effect of molecular weight and crystallinity on poly(lactic acid) mechanical properties. *J Appl Polym Sci* **1996,** 59 (1), 37-43 DOI: 10.1002/(Sici)1097-4628(19960103)59:1<37::Aid-App6>3.3.Co;2-7.

57. Besseling, R.; Weeks, E. R.; Schofield, A. B.; Poon, W. C. Three-dimensional imaging of colloidal glasses under steady shear. *Phys Rev Lett* **2007,** 99 (2), 028301 DOI: 10.1103/PhysRevLett.99.028301.

58. Laurati, M.; Masshoff, P.; Mutch, K. J.; Egelhaaf, S. U.; Zaccone, A. Long-Lived Neighbors Determine the Rheological Response of Glasses. *Phys Rev Lett* **2017,** 118 (1), 018002 DOI: 10.1103/PhysRevLett.118.018002.

59. Saltzman, E. J.; Yatsenko, G.; Schweizer, K. S. Anomalous diffusion, structural relaxation and shear thinning in glassy hard sphere fluids. *J Phys-Condens Mat* **2008,** 20 (24), 244129.

60. Ricci, J.; Bennin, T.; Xing, E.; Ediger, M. D. Linear Stress Relaxation and Probe Reorientation – Comparison of the Segmental Dynamics of Two Glassy Polymers During Physical Aging. Submitted.

61. Inoue, T.; Cicerone, M. T.; Ediger, M. D. Molecular Motions and Viscoelasticity of Amorphous Polymers near T_g. *Macromolecules* **1995,** 28 (9), 3425-3433.

62. Paeng, K.; Kaufman, L. J. Single Molecule Experiments Reveal the Dynamic Heterogeneity and Exchange Time Scales of Polystyrene near the Glass Transition. *Macromolecules* **2016,** 49 (7), 2876-2885 DOI: 10.1021/acs.macromol.6b00097.

63. Zhang, H.; Tao, K.; Liu, D.; Wu, K.; Wang, F.; Yang, J.; Zhao, J. Examining dynamics in a polymer matrix by single molecule fluorescence probes of different sizes. *Soft Matter* **2016,** 12 (35), 7299-306 DOI: 10.1039/c6sm01447j.

64. Lindsey, C. P.; Patterson, G. D. Detailed comparison of the Williams-Watts and Cole-Davidson functions. *Journal of Chemical Physics* **1980,** 73 (7), 3348-3357.

65. Medvedev, G. A.; Kim, J. W.; Caruthers, J. M. Prediction of the relationship between the rate of deformation and the rate of stress relaxation in glassy polymers. *Polymer* **2013,** 54 (24), 6599-6607 DOI: 10.1016/j.polymer.2013.10.008.